Research Article | Vol. 24, No. 14 | 11 Jul 2016 | OPTICS EXPRESS 15710
Optics EXPRESS

# Attenuation and diffusion produced by small-radius curvatures in POFs

**M. A. LOSADA,* A. LÓPEZ, AND J. MATEO**

*GTF, Aragón Institute of Engineering Research (i3A), Department of Electronic Engineering, University of Zaragoza, María de Luna 1, E-50018 Zaragoza, Spain*
* *alosada@unizar.es*

**Abstract:** Our aim is to characterize curvatures using a methodology previously applied to other localized disturbances in plastic optical fibers (POFs). The effects of several curvature radii and turn angles have been analyzed, so that for each condition, angular dependent attenuation and diffusion are obtained from experimental measurements to construct a matrix that accounts for the global effects of power loss and mode mixing introduced by the curvature over the angular power distribution. Power loss as a function of bend radius was calculated using the characteristic matrices and compared to experimental results to validate the model. This curvature model can be a useful tool to predict the impact of bends on transmission properties as is demonstrated in the example of a small network in a domestic environment.



**OCIS codes:** (060.0060) Fiber optics and optical communications; (060.2270) Fiber characterization; (060.2300) Fiber measurements; (060.2310) Fiber optics.

## References and links

1. M. A. Losada, I. Garces, J. Mateo, I. Salinas, J. Lou, and J. Zubia, "Mode coupling contribution to radiation losses in curvatures for high and low numerical aperture plastic optical fibers," J. Lightwave Technol. **20**(7), 1160–1164 (2002).
2. G. Durana, J. Zubia, J. Arrue, G. Aldabaldetreku, and J. Mateo, "Dependence of bending losses on cladding thickness in plastic optical fibers," Appl. Opt. **42**(6), 997–1002 (2003).
3. M. S. Kovacević and D. Nikezić, "Influence of bending on power distribution in step-index plastic optical fibers and the calculation of bending loss," Appl. Opt. **45**(26), 6675–6681 (2006).
4. J. Mateo, M. A. Losada, and J. Zubia, "Frequency response in step index plastic optical fibers obtained from the generalized power flow equation," Opt. Express **17**(4), 2850-2860 (2009).
5. M. A. Losada, J. Mateo, and J. J. Martinez-Muro, "Assessment of the impact of localized disturbances on SI-POF transmission using a matrix propagation model," J. Opt. **13**(5), 055406 (2011).
6. A. Esteban, M. A. Losada, J. Mateo, N. Antoniades, and A. López, "Effects of connectors in SI-POFs transmission properties studied in a matrix propagation framework," in *Proceedings of 20th Intl. Conf. on Plastic Optical Fibres and Applications* (2011), pp. 341–346.
7. M. Andrés, M. A. Losada, J. Mateo, and A. López, "Modelling the effects of small-radius curvatures in POFs," in *Proceedings of 24th Intl. Conf. on Plastic Optical Fibres and Applications* (2015).
8. M. A. Losada, J. Mateo, and A. López, "Matrix model of optical power propagation in plastic optical fibres," in *Proceedings of 12th Intl. Conf. on Transparent Optical Networks* (IEEE, 2010), paper We.C3.3.
9. J. Mateo, M. A. Losada, I. Garcés, and J. Zubia, "Global characterization of optical power propagation in step-index plastic optical fibers," Opt. Express **14**(20), 9028–9035 (2006).
10. D. Richards, M. A. Losada, N. Antoniades, A. López, J. Mateo, X. Jiang, and N. Madamopoulos, "Modeling methodology for engineering SI-POF and connectors in an avionics system," J. Lightwave Technol. **31**(3), 468–475 (2013).
11. M. A. Losada, J. Mateo, I. Garcés, J. Zubia, J. A. Casao, and P. Pérez-Vela, "Analysis of strained plastic optical fibers," IEEE Photonics Technol. Lett. **16**(6), 1513–1515 (2004).
12. A. López, M. A. Losada, and J. Mateo, "Simulation framework for POF-based communication systems," in *Proceedings of the 17th Intl. Conf. on Transparent Optical Networks* (IEEE, 2015), pp 1–4.
13. N. Antoniades, M. A. Losada, J. Mateo, D. Richards, T. K. Truong, X. Jiang, and N. Madamopoulos, "Modeling and characterization of SI-POF and connectors for use in an avionics system," in *Proceedings of 20th Intl. Conf. on Plastic Optical Fibres and Applications* (2011), pp. 105–110.

#260198 http://dx.doi.org/10.1364/OE.24.015710
Journal © 2016 Received 29 Feb 2016; revised 28 May 2016; accepted 1 Jun 2016; published 1 Jul 2016

Optics EXPRESS

## 1. Introduction

The layout of POFs for their usual short-range applications in reduced environments as cars, planes and houses requires a number of bends that often have very small radii. Although POFs are more resistant to bending loss than glass fibers, reported curvature losses can reach several dBs for radii below 20 mm depending on the fiber index profile, its numerical aperture and the curvature configuration [1]. Moreover, it is reasonable to expect that curvatures introduce not only angle-dependent power loss but also power transfer among modes (mode mixing) both with an impact on fiber bandwidth. Thus, a model that accounts for power loss and mode mixing caused in small bends is needed to incorporate the effects of curvatures into network simulations. In this line, ray-tracing models that account for mode mixing in curvatures are able to give good predictions at the cost of long calculation time [2]. Another approach based on segmentation of the time-independent power flow equation is also able to estimate the changes in the angular power distribution produced by a given curvature but so far it has only been tested for radii larger than 10 cm [3].

In previous works, we showed that a POF can be modelled by a characteristic matrix to describe the amount of power in a given angle that is transferred to another angle for each temporal frequency and where the optical power distribution transmitted through the fiber is described as a function of propagation angle and frequency. The characteristic matrix for an infinitesimal fiber length is a tri-diagonal matrix calculated using the fiber angular attenuation and diffusion functions that were obtained from experimental measurements [4]. This approach was later extended to describe passive components that produce localized disturbances over the optical power propagated through the fiber [5]. The device introduces localized power loss and strong mode coupling as the power transfer is accomplished in a very short distance, not only between adjacent modes or angles, but also to others further away or even to radiating modes. In fact, we showed that connectors can be modelled using a square matrix obtained as a tri-diagonal matrix but elevated to a high exponent to account for the greater and localized changes they impose in optical power distribution. The elements of this tri-diagonal matrix are also calculated from the angular attenuation and diffusion that underlie the global power loss and mode mixing produced by the device [6]. To obtain these functions, we devised a method based on the comparison of experimental output far field patterns (FFPs) measured with and without the disturbance and for different launching angles [7].

Here, we analyze the effects on a 1 mm step-index POF of small bends whose radii range from 3 to 35 mm, and for two turn angles: 360° and 90°. These turn angles have been selected as fiber loops (360° turns) are often made to store the fiber in small receptacles, while 90° turns are a good representation of the shape fibers take around nooks and corners that are frequent in houses. The range of bend radii has been chosen to cover the span of curvatures that are likely to occur in the installation of domestic links. Our final aim is to provide a new tool that can be integrated into our proposed matrix framework to model light propagation in POF networks [8]. In this way, a POF link can be simulated by the product of several matrices that model different fiber lengths, the connectors that join them, and also the bends necessary to install the fiber in a realistic environment.

The paper is organized as follows: First, the methodology to obtain the mode dependent attenuation and diffusion from the experimental radial profile scans with and without the bends is described. Next, we show the attenuation and diffusion obtained for all conditions. Also, we perform a study of the variation of the curvature effects as a function of time to assess the stability of the model. Then, the corresponding matrices calculated from the curvature characteristic functions are displayed. These matrices are used to validate the model comparing its predictions to measured power loss versus curvature radius. Last, a case example is implemented to illustrate how this curvature characterization can be integrated in the POF matrix model and to show the consequences of bending in a domestic network. Finally, we summarize our results and emphasize our conclusions.

Optics EXPRESS

## 2. Methods

In the first subsection, the experimental set-up to obtain the FFPs scanning the input angle is described and the measurements of FFP radial profiles obtained for bent fibers are shown. Next, we explained how the comparison of these experimental radial profiles to those measured for a straight fiber can be used to obtain the free parameters of a model based on a characteristic matrix postulated to describe the total power loss and mode mixing produced by the curvature. The fiber tested was an ESKA PREMIER from Mitsubishi that is a step index PMMA POF of 1 mm of diameter. For the experiments, we used fiber samples of 2.5 meters as this length was sufficient to ensure the minimum changes in fiber position through the whole set of measurements. We tested 360° and 90° turns with radii of 3, 6, 13, 25 and 35 mm.

### *2.1 Experimental set-up and measurements*

FFPs were obtained injecting a collimated beam directly into the fiber input end. This end was placed on the center of a motorized rotary mount to vary the input or launching angle from −40° to 40° in 1° steps as described in [5]. The images of the output FFPs reflected from a white screen were recorded by a cooled CCD. From each FFP image, the radial profile was extracted to provide a measurement of the optical power as a function of the FFP output angle relative to the fiber axis. All the angles in this paper are external to the fiber. The experimental conditions for these measurements were specifically designed to apply the curvature under test without introducing further bending of radii comparable to the one under test in other sections of the fiber. The FFP-scans were recorded first for the straight fiber to serve as a reference, and then for the fiber with the curvature, starting first from the largest radius down to the smallest one. Independent series were taken for the 360° and 90° turns. The curvatures were applied at 20 cm from its output end using a mandrel that was a pile of cylinders with different radii starting from 35 mm at the base and decreasing to 3 mm at the top step. This curvature tower was the same used in [1] and is depicted in Fig. 1, as well as the two configurations used to test the 90° and 360° curvatures. The fiber was kept straight in the 20 cm previous to the curvature tower whose lateral position and height were changed using poles to avoid bending the fiber in other axes.

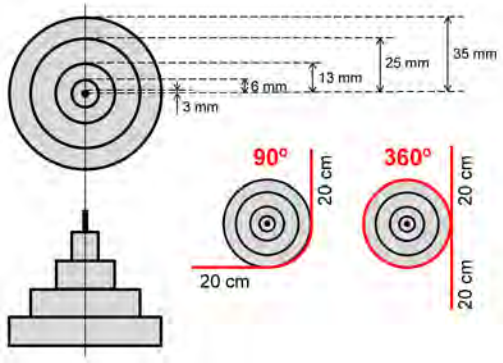


Fig. 1. Schematic of the curvature tower showing the set of radii and turn angles considered.

A control experiment to assess the influence of the turn sign (clockwise or anti-clockwise) was performed but the results did not show systematic differences and all the results were pooled together. Also, measurements for negative and positive launching angles for the same fiber were considered as independent measurements.

Figure 2 shows some experimental measurements that will be later used to determine the characteristic matrix for the corresponding curvature. These measurements were obtained for a fiber segment bent a complete turn and a quarter of a turn with radii of 35 and 6 mm,

Optics EXPRESS

respectively. Each image corresponds to a matrix, **P** where all the FFP radial profiles obtained for a launching angle scan are displayed on a single plot. Each column shows the FFP radial profile obtained for a given input or launching angle (horizontal axis) as a function of the FFP output angle (vertical axis). Red indicates the highest power while blue is the lowest. All images have been normalized to the maximum value that was found in the measurement for 35 mm and 360°. They illustrate how bending produces power loss at high angles for the smaller radii and also introduces some power spread among angles that is revealed by the slight widening of the patterns which is more evident in the diagonals. Also, notice that loss at low angles is higher for the 90° than for the 360° turn.

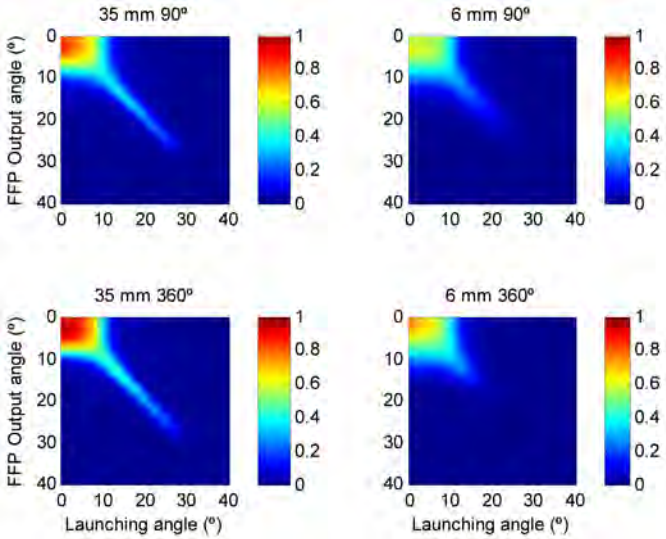


Fig. 2. Experimental FFP radial profiles: bend radius of 35 mm (left) and 6 mm (right) for 90° and 360° turn angles.

### *2.2 Estimation of the characteristic functions*

We assume that the global effect of the curvature can be mathematically modeled as a linear system so that the output power at a given propagation angle can be written as a linear combination of the power at that and other angles and thus, the angular power distribution after the bend in vector form can be obtained multiplying the characteristic matrix by the power distribution before the bend. The experimental FFP radial profiles measured with and without the bend provide a representation of the angular power distribution after and before the curvature, respectively. Thus, their relationship is the following:

$$\mathbf{P}^{\mathbf{C,R}} = \mathbf{M}^{\mathbf{C,R}} \cdot \mathbf{P}^{\mathbf{REF}}, \tag{1}$$

where $\mathbf{M}^{\mathbf{C,R}}$ is the characteristic matrix for a curvature of angle C (360° or 90°) and radius R, and $\mathbf{P}^{\mathbf{C,R}}$ and $\mathbf{P}^{\mathbf{REF}}$ are the matrices of the FFP radial profile scans measured with and without the curvature, respectively.

To obtain the curvature characteristic matrix, we start from a tri-diagonal matrix, $\mathbf{M_0}^{\mathbf{C,R}}$. Its elements are calculated from the attenuation function: $\alpha$ ($\theta$) in Np/m, that describes power loss for each angle outer to the fiber, $\theta$, and the diffusion coefficient: $d_0$, in rad$^2$/m, that is the power transferred to adjacent angles and underlies mode mixing, as:

Optics EXPRESS

$$M_{0_{k,k-1}}^{C,R} = d_0 \frac{2k-1}{2k} \frac{\Delta z}{\Delta \theta^2}$$
$$M_{0_{k,k}}^{C,R} = \exp(-\Delta z \cdot \alpha(k \cdot \Delta\theta)) - 2d_0 \frac{\Delta z}{\Delta \theta^2}, \quad (2)$$
$$M_{0_{k,k+1}}^{C,R} = d_0 \frac{2k+1}{2k} \frac{\Delta z}{\Delta \theta^2}$$

where $\Delta\theta$ = 0.005 rad and $\Delta z$ = 0.001 m are the infinitesimal angular and axial coordinates [4].

To model the global effects of the curvature that are localized but intense, its characteristic matrix $\mathbf{M^{C,R}}$, is calculated as the power of this basic matrix:

$$\mathbf{M^{C,R}} = \left(\mathbf{M_0^{C,R}}\right)^N, \quad (3)$$

where $N$ is a very large integer that in our case was fixed to 10000. The exact value of $N$ is arbitrary, provided it is large enough to account for the effects of the curvature. If this value is changed, the obtained values of $\alpha$ ($\theta$) and $d_0$ will change accordingly but the resulting global characteristic matrix will be the same.

A good approximation of the angular attenuation function for the curvature can be directly obtained from a pair of experimental FFP radial profile scans while the diffusion is estimated fitting the model to the experimental measurements. We found that a good fit was reached with a constant diffusion as we did in the case of connector characterization [6]. In both cases, the high variability of the measurements prevents further refinement using a diffusion function of several fitting parameters. Thus, the expressions in Eq. (2) to calculate the elements of the tri-diagonal matrix were given specifically for a constant diffusion.

As the sum of all the elements of a row in matrix $\mathbf{P}$ is related to the total power for the corresponding propagation angle, the ratio of this sum for the reference matrix $\mathbf{P^{REF}}$, relative to the same sum for the matrix with the curvature $\mathbf{P^{C,R}}$ provides the power change at that angle introduced by the curvature under test:

$$\alpha_{C,R}(\theta) \to \boldsymbol{\alpha}_{\mathbf{j}}^{\mathbf{C,R}} = 10 \cdot \log_{10}\left(\frac{\sum_i \mathbf{P_{i,j}^{REF}}}{\sum_i \mathbf{P_{i,j}^{C,R}}}\right). \quad (4)$$

Then, the diffusion constant, $d_0$, for each measurement was fitted to minimize the following cost function:

$$F = \left\| \mathbf{P^{C,R}} - \mathbf{M^{C,R}} \times \mathbf{P^{REF}} \right\|, \quad (5)$$

where $\mathbf{M^{C,R}}$ was calculated using Eq. (3) and introducing the attenuation function obtained using Eq. (4) for the corresponding measurement and a trial diffusion coefficient [6].

Notice that although the infinitesimal matrix is obtained from attenuation and diffusion, we do not try to model the physical propagation path of light throughout the bend. We use this approach as an efficient way to model the global behavior of the curvature.

## 3. Results

### *3.1 Curvature attenuation and diffusion effects*

Figure 3 shows the attenuation and diffusion values obtained for all conditions tested. Attenuation is the average of at least eight measurements. The middle graph shows the overall diffusion as a function of the curvature radius for the two turn angles, also obtained averaging the values for all individual measurements. Error bars show the standard deviation for the diffusion and for the attenuation illustrating their high variability. The origin of this variability is the impact on power distribution of factors such as fiber termination, position, etc.

Optics EXPRESS

The attenuation curves show a relative flat base at lower propagation angles that rises steeply from a given propagation angle. This cut-off angle (shown as a triangle) is lower the smaller the curvature radius, and higher for the 90° turns (right graph) than for the 360° turns (left graph) of the same radius. From the cut-off angle, attenuation rises linearly with slopes that are steeper for 360° than for 90° curvatures. In general, the attenuation for low angles is higher for the 90° turns than for the 360° turns as was also visible in the images shown in Fig. 2. Figure 3 also shows that the value of the diffusion is higher for 90° than for 360° turns. In both cases, diffusion is higher for the smaller bends, decreasing slightly with increasing radii. The order of magnitude of the diffusion for curvatures is relative small compared with that of the fiber and connectors [6, 9]. In fact, it is about three times lower than the value found for polished connectors [10].

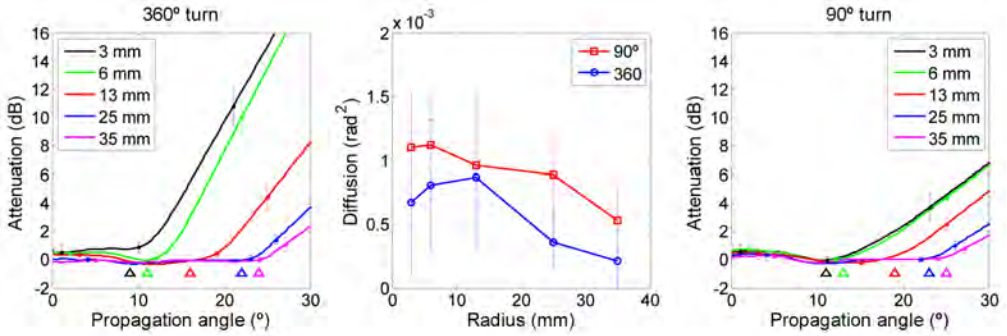


Fig. 3. Attenuation as a function of propagation angle obtained for different curvature radii and turn angles of 360° (left) and 90° (right); overall diffusion as a function of bend radius for 360° and 90° turns (center).

Thus, our findings reveal that curvatures act as spatial filters that reduce the optical power transmitted above a given angle. This filtering is more effective for the complete turn than for the quarter of a turn.

### *3.2 Permanence of curvature effects*

In previous works, we have assessed and quantified permanent changes in fiber propagation properties produced by extensive long-duration strains applied over the fiber [11]. Here, we repeated the characterization procedure after leaving the fiber installed at the curvature tower for extended periods of time to determine if there were changes in its attenuation and diffusion. We kept several fiber segments bent a 360° turn over the smallest radius in the curvature tower (3 mm) for periods longer than 15 hours. Our results do not reveal changes in the attenuation as is evident in the left graph of Fig. 4 where several of these individual measurements have been represented. In the right graph, the diffusion is shown. Different colors in both plots indicate measurements corresponding to different fiber segments. The black line is the average value for the diffusion for the 3 mm 360° turn with its standard deviation to allow assessment of the differences. The circles show the initial value of the diffusion coefficient and the squares the value obtained after waiting some time specified on the horizontal axis. The figure shows that the diffusion coefficient value estimated after a time was systematically lower than its initial value. However, these small decrements of diffusion are well below the standard deviation also plotted in the figure.

Optics EXPRESS

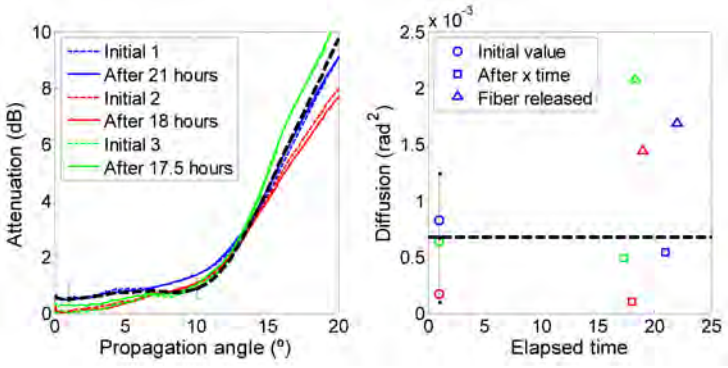


Fig. 4. Temporal variation of the attenuation (left) and the diffusion (right) for a 3-mm radius and 360° turn.

The characterization procedure was also carried out after un-bending and straightening each fiber segment. The differences between the obtained attenuation and the reference curves, not shown in order to simplify the graph, are below the standard deviation so that we can conclude that the changes over the angular attenuation of the released fiber are not relevant. However, the values of the diffusion coefficient obtained after releasing the fiber, shown as triangles of the color of the corresponding measurement, are significantly higher than those obtained just before. This increase of diffusion can be related to the breakage of molecular bonds when the fiber is straightened after it has been bend for a long time. These findings confirm that it is not advisable to re-use fibers once they have been bent. A similar behavior was obtained after bending the fiber 90° and 3 mm.

### *3.3 Curvature characteristic matrices*

The curvature characteristic matrices, $\mathbf{M}^{C,R}$, are displayed in Fig. 5 for radii of 35 and 6 mm and both turn angles. The images have been normalized to the maximum of all displayed matrices (located on the matrix for 360° and 35 mm) to visualize their differences.

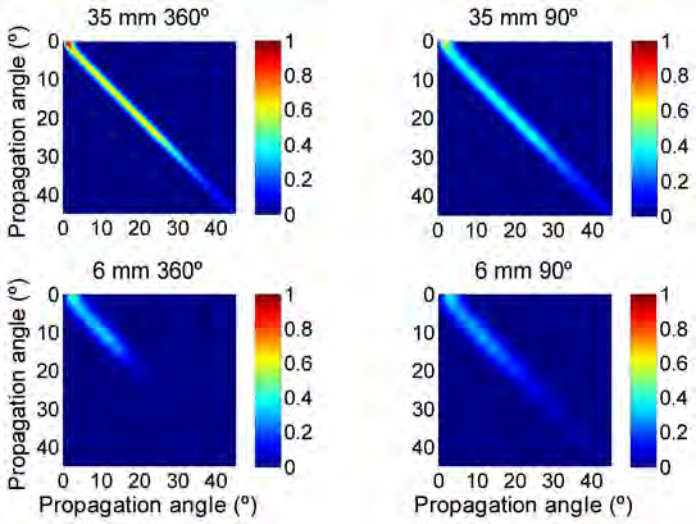


Fig. 5. Curvature characteristic matrices: 360° turn (left) and 90° turn (right).

The characteristic matrices show a nearly diagonal pattern, which is shorter for smaller radii due to the higher power loss at higher angles. The cause of power loss at a given angle can be coupling to other modes or radiation but our approach does not provide this

Optics EXPRESS

information. The diagonal width describes the overall power diffusion which is relatively low. This image representation demonstrates how the effect of curvatures is filtering out power at high propagation angles, more restrictively for 360° than for 90° bends due to their lower cut-off angles and higher attenuation slopes. The filter selectivity is yet enhanced for the 360° turn whose matrix shows lower attenuation at low angles and less mode mixing than that corresponding to the 90° turn. This fact is also evident in Fig. 1 where we remarked how the radial profiles measured for low angles (left hand corner of the patterns) show higher values for 360° than for 90° turns. The higher mode mixing for the 90° turn is consistent with our previous finding that higher bending losses are related to the number of curved-to-straight fiber transitions [1].

To emphasize our findings and to show that the overall effect of a curvature in which only a few centimeters of fiber are involved is comparable to those of power propagation through a relatively long straight fiber, Fig. 6 shows the characteristic matrix of a 10 meter GH fiber and those obtained for 360° and 90° bends of 3 mm radius. Images are normalized to the maximum value of the three that, in this case, is in the characteristic matrix for 360° and 3 mm. Optical power transmission through the fiber imposes a filtering of power at high angles similar to that of the curvature but with substantially more mode mixing, particularly at low angles. In fiber propagation, the higher diffusion and attenuation at lower and middle angles increase the global power loss and mode mixing compared to bends. The shapes of the curvature matrices are closer to that of a diagonal matrix so that they behave as a highly selective angular filter that removes power from a cut-off angle while confining power at lower angles with only slight loss and a little spread.

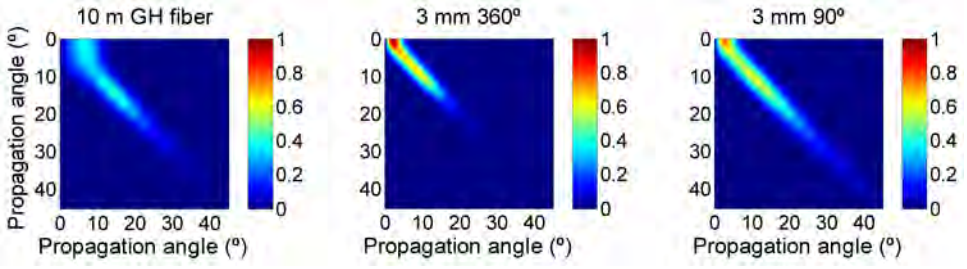


Fig. 6. Curvature characteristic matrices for 3-mm bend radius: 360° turn (center) and 90° turn (right). Comparison with characteristic matrix of 10 meters of fiber without bending (left).

### *3.4 Validation experiment*

We tested the model by comparing its predictions of total power loss to measurements obtained using a very wide LED source. We measured the curvature loss introduced by 360° bends in several 2.5 meter segments of GH fiber near their output end using a 660 nm LED to inject power. These fiber segments were different from those used in the characterization procedure. In addition, the FFP radial profile using this LED as the launching source was first measured for the straight fiber segment and put in vector form as a function of the propagation angle: $\mathbf{p}^{\mathbf{LED}}$. This distribution can be used to predict the angular power distribution after the fiber is bent using the characteristic matrix:

$$\mathbf{p}^{360°,R} = \mathbf{M}^{360°,R} \cdot \mathbf{p}^{\mathbf{LED}}. \tag{6}$$

The total power for a given angular power distribution can then be obtained as:

$$P_{Total} = \sum_k p_k \cdot \sin\left(k \cdot \Delta\theta\right) \cdot \Delta\theta. \tag{7}$$

In Fig. 7, the experimental results are shown as power loss in dB with their standard deviation to demonstrate their good agreement with model predictions.

Optics EXPRESS

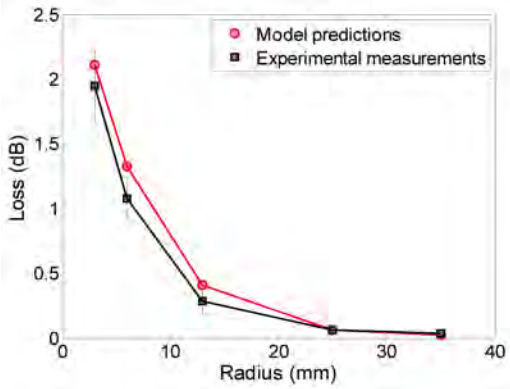


Fig. 7. Bending loss as a function of radius: model predictions (red), experimental measurements (black).

### *3.5 Integration into the matrix simulation environment*

The curvature matrix can be integrated into the POF propagation matrix toolbox and used to incorporate the effects of bends at different positions the link [12]. The angular low-pass shape of the curvature matrices allows us to predict an enhancement of transmission capability in the presence of bends that filter the slower modes out of the power distribution similar to that found for other devices [5,13]. However, this assumption cannot be generalized because power distribution in POFs shows a strong dependence on launching aperture and fiber length. Therefore, to illustrate the impact of curvatures on transmission properties in a likely scenario, we consider a 20-meter POF link where it is necessary to bend the fiber around a corner. We contemplated two possible implementations depending if the curvature is closer to the emitter or to the receiver. The schematic depicted in Fig. 8 shows the two configurations implemented: a) and c), as well as configuration b) with the fiber straight to serve as a reference. To assess the influence of launching numerical aperture (NA), the analysis has been performed for two different sources.

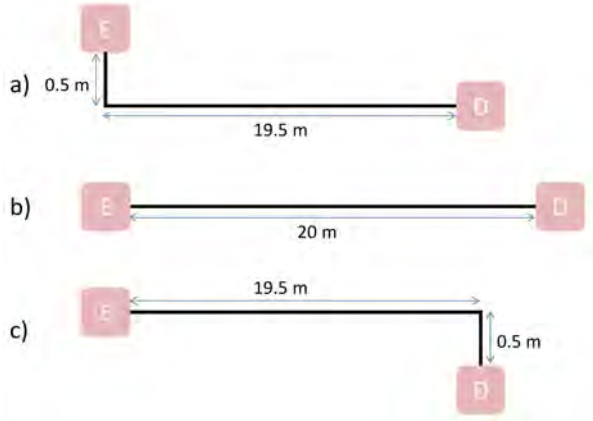


Fig. 8. Twenty-meter POF link: a) with a corner at 0.5 m from the emitter; (b) no corner; (c) with a corner at 0.5 m from the receiver.

A curvature of 90° and 6 mm radius has been used to describe bending the fiber around a corner, so the characteristic matrix used is $\mathbf{M}^{90°,6mm}$. In our approach, vectors represent the angular power distributions at different points in the link and matrices describe the diffusion and loss introduced by different fiber lengths or by curvatures. The configurations shown in Fig. 8 are implemented by the following matrix products using a simplified notation where the

Optics EXPRESS

frequency dependence in the characteristic matrices for different fiber lengths and in the power distribution vectors is not explicitly shown:

$$\begin{aligned} &\text{a)}\ \mathbf{p}_D = \mathbf{M}_{19.5m} \cdot \mathbf{M}^{90°,6mm} \cdot \mathbf{M}_{0.5m} \cdot \mathbf{p}_E \\ &\text{b)}\ \mathbf{p}_D = \mathbf{M}_{20m} \cdot \mathbf{p}_E \\ &\text{c)}\ \mathbf{p}_D = \mathbf{M}_{0.5m} \cdot \mathbf{M}^{90°,6mm} \cdot \mathbf{M}_{19.5m} \cdot \mathbf{p}_E, \end{aligned} \tag{8}$$

where $\mathbf{p}_E$ is the source angular distribution in vector form, and $\mathbf{p}_D$ the transmitted power distribution that reaches the detector. $\mathbf{M}_L$ is the propagation matrices that account for power loss and mode coupling caused by $L$ fiber meters (in this case, $L$ is 0.5, 19.5 or 20 m). Both the fiber propagation matrix and the power distribution have dependences on the angle and the frequency, while the curvature matrix only has angular dependence. The power distribution vector carries not only angular but also frequency information and can be used to obtain not only the angular power distributions but also the transfer function. In Fig. 9, the amplitude of the transfer functions measured at the detector is compared for the three configurations. The left graph shows the simulation results when the source has a wide emission pattern such as a LED (with a FWHM of 30°) and the one on the right for a narrower source such as a VCSEL (10°). As all matrices are independent on the input conditions, they do not have to be re-calculated to evaluate the link when the source is changed.

When using the LED as optical source, the bend increases bandwidth for both deployment configurations. This increase of over 30% of its reference value is achieved by the filtering out of the power at higher angles with slower modes. The cost of this bandwidth increase is a relative small power loss: 1.1 dB for configuration a) and 1.2 dB for configuration c) relative to reference case b). For the VCSEL, however, the bend degrades the performance when it is near the source, while there is slight improvement when it is near the receiver. Power losses are 0.44 and 0.37 dB, respectively for configurations a) and c). They are lower with this narrow launching conditions that confine of power at lower angles which, as we have shown, are much less affected by bending.

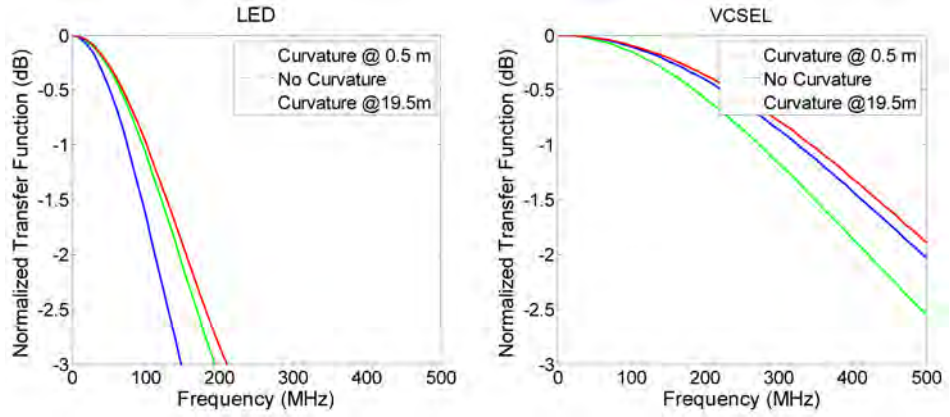


Fig. 9. Normalized transfer function obtained at the detector for a LED (left) and a VCSEL (right) for the three configurations tested.

## 6. Conclusions

In this paper, we have assessed the effects of several small-radius curvatures for a quarter of a turn (90°) and a complete turn (360°) obtaining their characteristic matrices. Results show how curvatures produce intense power loss for angles higher than a cut-off angle that decreases with the bend radii and is higher for 90° turn angles. Mode mixing produced at the

Optics EXPRESS

bend is slight so that, according to our work, small radius curvatures have the effect of an angular low-pass filter that is more selective for 360° than for 90° turns. Therefore, curvatures in a POF link can enhance transmission capacity as they filter out the slowest modes from the optical power distribution depending on their position, the launching conditions, etc. The curvature characteristic matrix can predict changes produced over any power distribution and thus, its integration as a new block of the propagation matrix framework will provide more realistic simulations of POF network designs before their deployment.

## Acknowledgments

This work has been funded by the Fondo Europeo de Desarrollo Regional (FEDER) and by the Spanish Ministerio de Economía y Competitividad under project TEC2015-63826-C3-3-R (MINECO/FEDER).